Applied Catalysis B: Environmental 119–120 (2012) 146–155

Contents lists available at SciVerse ScienceDirect

Applied Catalysis B: Environmental

journal homepage: www.elsevier.com/locate/apcatb

Effect of Au supported TiO_2 with dominant exposed {0 0 1} facets on the visible-light photocatalytic activity

Shuying Zhu, Shijing Liang, Quan Gu, Liyan Xie, Jixin Wang, Zhengxin Ding, Ping Liu*

Research Institute of Photocatalysis, State Key Laboratory Breeding Base of Photocatalysis, Fuzhou University, Fuzhou 350002, PR China

ARTICLE INFO

Article history:
Received 24 November 2011
Received in revised form 16 February 2012
Accepted 20 February 2012
Available online 27 February 2012

Keywords:
TiO_2 nanosheets
Au nanoparticles
{0 0 1} facets
Plasmonic photocatalyst
Visible light

ABSTRACT

Novel visible-light-driven plasmonic photocatalyst Au/TiO_2 nanosheets with a high percentage of exposed {0 0 1} facets were fabricated by hydrothermal treatment of tetrabutyl titanate and hydrofluoric acid, followed by the polyol reduction process (denoted by Au/TiO_2-0 0 1). The prepared samples were characterized by transmission electron microscopy, X-ray diffraction, X-ray photoelectron spectroscopy, N_2-sorption, UV-vis diffuse reflectance spectroscopy, and photoluminescence spectra. The variations of photoelectric response after depositing Au nanoparticles (NPs) on TiO_2-0 0 1 nanosheets were investigated by the photoelectrochemical experiment. The results display that the Au NPs with average diameter of ca. 5 nm were deposited on (0 0 1) facet of TiO_2 nanosheets in the form of metallic state. The samples exhibited a strong absorption in the visible light region due to the surface plasmon resonance (SPR) effect of Au NPs. For the photocatalytic degradation of rhodamine B (RhB) in aqueous solution, the Au/TiO_2-0 0 1 showed superior photocatalytic activities compared with bare TiO_2-0 0 1 and other Au deposited photocatalysts, such as Au/P25 (Degussa TiO_2), Au/anatase TiO_2, and Au/rutile TiO_2. The enhanced photocatalytic activities can be explained by its unique morphology, larger surface area, and smaller crystallite. Meanwhile, TiO_2 dominated {0 0 1} facets with higher electron mobility and better adsorption of pollutant molecule may be another reason for the higher photocatalytic activity. In addition, the Au NPs are believed to play an essential role in enhancing the photoreactivity because they are able to generate photoelectrons and enhance the visible light absorption intensity. The effects of the Au content, the calcination temperature of TiO_2-0 0 1, the supporter, and the reaction atmosphere on photocatalytic activities were investigated in detail. The decomposition mechanism of RhB over Au/TiO_2-0 0 1 under visible light irradiation and the active species in the photocatalytic process had also been discussed. It is hoped that our work could render guided information for steering toward the design and application of noble metal/semiconductor nanocompositions with high visible-light photocatalytic activity.

1. Introduction

It has been widely accepted that the catalytic activity of a semiconductor-based photocatalyst can be influenced by its surface structure which is directly exposed to the reaction media [1,2]. Recently, surface chemists have made great efforts to study of the chemical properties of defined crystal planes on TiO_2 [3–5]. Anatase TiO_2 has attracted a lot of attention owing to its outstanding photocatalytic performances. Both theoretical and experimental studies indicated that the average surface energies of anatase TiO_2 are 0.90 J/m^2 for (0 0 1), 0.53 J/m^2 for (1 0 0), and 0.44 J/m^2 for (1 0 1), respectively. It has been reported that the (0 0 1) facet of anatase TiO_2 nanosheets exhibited much higher activity compared with the thermodynamically stable (1 0 1) facet [4–9]. Han et al. demonstrated that nanosized anatase TiO_2 single crystals with up to 89% exposed highly energetic {0 0 1} facets showed an excellent photodegradation efficiency toward methyl orange [3]. Moreover, micro-sized TiO_2 crystallites with a high percentage of {0 0 1} facets synthesized by Liu et al. also showed a highly photocatalytic activity for H_2 evolution [10]. They may be ascribed to the low density of defects on TiO_2 {0 0 1} facets, which could reduce the recombination rate of photogenerated electron–hole pairs at the grain boundaries. Although increasing the percentage of {0 0 1} facets would efficiently enhance the photocatalytic activity, TiO_2 is only drived by ultraviolet light, accounting for only ca. 4% of the solar spectrum. In view of the efficient utilization of visible light, it is necessary to develop a novel TiO_2-based photocatalysts with a high percentage of {0 0 1} facets which can work efficiently under a wide range of visible-light irradiation.

In previous reports, TiO_2 doped with non-metal or metal can create localized/delocalized states in the band gap and thus extend

* Corresponding author. Tel.: +86 591 83779239; fax: +86 591 83779239.
E-mail address: liuping@fzu.edu.cn (P. Liu).

0926-3373/$ – see front matter © 2012 Elsevier B.V. All rights reserved.
doi:10.1016/j.apcatb.2012.02.020

its optical absorption to the visible region. For instance, Xiang et al. [11] reported that nitrogen and sulfur co-doped TiO_2 nanosheets with exposed {0 0 1} facets exhibited highly photocatalytic activity toward 4-chlorophenol under visible light irradiation. Zong et al. found that F, N co-doped TiO_2 with dominant exposed {0 0 1} facets showed highly photocatalytic water oxidation under visible light [12]. However, the dopants may cause the charge carriers accelerated recombination and lower stability of the doped materials. In addition, despite the fact that adsorbed dye molecules on the surface of the photocatalysts can increase their photoabsorption abilities, the stable and efficient dyes are rare. Therefore, the development of undoped and stable TiO_2-based visible-light drived photocatalysts still remains challenging so far.

Noble metals have attracted significant interest due to their unique electronic, optical, and magnetic properties. It is reported that noble metals (such as Au, Ag, and Pt) can strongly absorb visible light due to their surface plasmon resonance (SPR) effect [13,14]. Thereafter, the noble mental nanoparticles deposited on TiO_2 were considered as an approach to extend the spectral response of TiO_2 to visible light [15–17]. For example, Chen et al. reported that Au/TiO_2 plasmonic photocatalyst in water splitting showed a highly photocatalytic activity under visible light irradiation [18]. Zheng et al. found that Au@TiO_2 exhibited a high yield and selectivity for the catalytic oxidation of benzene to phenol in aqueous phenol [19]. For the synthesis of noble-metal decorated TiO_2, some approaches have been reported, including the conventional impregnation, the deposition-precipitation, the photodeposition, and sol–gel methods [20–23]. However, due to the fast rate of particle formation, most of the common synthetic methods are relatively simple but not feasible to produce noble metal nanoparticles with small and uniform size. The aggregation will reduce the surface area and utilization ratio of noble metal NPs [24]. Furthermore, the photocatalytic activities of noble-metal-semiconductor nanocomposites are strongly related to their physical characteristics, such as size [25–29] and shape [30–34]. For Au nanoparticles, their catalytic activities are very sensitive to their sizes. The smaller the size, the higher the catalytic activity [35,36]. In addition, researchers have focused on loading noble metal nanoparticles on the common TiO_2. However, the work on the preparation of visible-light-responsive anatase TiO_2 with dominant {0 0 1} facets using the SPR effect of noble metal has been rarely investigated up to now. Therefore, it is desirable to develop a facile and controllable method to prepare nanoscale, uniform, and well-disperse noble mental particles on TiO_2 with dominant {0 0 1} facets.

Herein, a novel method has been developed to deposit uniform Au NPs on TiO_2 nanosheets with high exposed {0 0 1} facets for the first time. The physiochemical properties of the products have been characterized in detailed. The variations in the photoabsorption ability and photoelectric response of TiO_2-0 0 1 before and after Au NPs deposited are also investigated by UV-vis DRS and the photoelectrochemical experiment, respectively. The photocatalytic activities of Au/TiO_2-0 0 1 nanosheets are evaluated by degrading rhodamine B (RhB) under visible light irradiation ($420 < \lambda < 760$ nm). Compared with bare TiO_2-0 0 1, N-TiO_2, and other Au deposited photocatalysts such as Au/P25, Au/anatase TiO_2, and Au/rutile TiO_2, the as-prepared Au/TiO_2-0 0 1 exhibits the highest photocatalytic activity. Possible reasons for the enhancement of photocatalytic performance are also discussed. Furthermore, the effects of the Au deposition level, the calcination temperature of TiO_2-0 0 1, the supporters, and the reaction atmosphere on photocatalytic activities are investigated in detail. The decomposition mechanism of RhB over Au/TiO_2-0 0 1 under visible light irradiation and the active species in the photocatalytic process have also been discussed and proposed.

2. Experimental

2.1. Materials

Tetrabutyl titanate ($Ti(OBu)_4$, 98%), hydrofluoric acid (47%), tetrachloroauric acid tetrahydrate, polyvinylpyrrolidone (PVP, $M_w = 40$ K), ethylene glycol (EG) and sodium sulfate used in these studies were purchased from Sinopharm Chemical Reagent Co. Ltd., sodium sulfocyanate was obtained from Alfa Aesar, and terephthalic acid was purchased from Acros Chemical Co. All of the reagents were analytical grade and used without any further purification.

2.2. Synthesis of TiO_2 nanosheets

Anatase TiO_2 nanosheets with exposed {0 0 1} facets (designated as TiO_2-0 0 1) was synthesized by a previously reported method [3]. In a typical experimental procedure, 25 ml of $Ti(OC_4H_9)_4$ and 3 ml of hydrofluoric acid solution with a concentration of 47 wt.% were mixed in a dry Teflon-lined autoclave with a capacity of 100 ml at ambient temperature. The mixture solution was stirred at the room temperature for 30 min, and then treated by hydrothermal reaction at 180 °C for 24 h. After being cooled down to room temperature, the white precipitate was collected by high-speed centrifugation and washed with distilled water and ethanol for several times. Finally, the sample was dried in an oven at 80 °C for 6 h.

2.3. Preparation of the Au–TiO_2 nanosheets hybrid

The Au supported TiO_2 nanosheets (designated as Au/TiO_2-0 0 1) were prepared by the sulfide-mediated polyol process with some modifications [37]. Typically, 0.6 g TiO_2-0 0 1 was first suspended into 80 ml of ethylene glycol (EG) under vigorous magnetic stirring at room temperature. Then, the suspension was heated at 150 °C on oil bath with constant and vigorous stirring. After 40 min of preheating, a flow of high-purity argon was introduced via a polytetrafluoroethylene tube to completely remove O_2 in the system. After that, 0.084 g of a sodium sulfocyanate and 15 ml of polyvinylpyrrolidone added in the above EG solution and finally a desired amount of H_2AuCl_4 solution (10 mg/ml) was quickly injected into system. The solution turned to purple after 20 min of heating, and then was quenched by placing the reaction flask in an ice-water bath. During the process, the solution was bubbled constantly by high-purity argon. The final sample was obtained and washed with acetone and deionized water to remove excess EG and PVP. A series of Au supported TiO_2 nanosheets labeled as Au_x/TiO_2-0 0 1 (Au wt.% = 0.5, 1.0 and 2.0, respectively) with different amount of Au were obtained by the adding desired amount of H_2AuCl_4 solution in the reaction system. For comparison, the Au supported P25, anatase and rutile TiO_2 nanoparticles were also prepared by the same method.

2.4. Characterization

Transmission electron microscopy (TEM) images were recorded using a JEOL model JEM 2010 EX microscope at an accelerating voltage of 200 kV. The X-ray diffraction (XRD) measurements were performed on a Bruker D8 Advance X-ray diffractometer using Cu $K\alpha_1$ radiation ($\lambda = 1.5406$ Å). The Brunauer–Emmett–Teller (BET) surface area was measured with an ASAP2020M apparatus (Micromeritics Instrument Corp.). The elemental composition of as-prepared samples was analyzed by X-ray photoelectron spectroscopy (XPS, VG, Physical Electrons Quantum 2000 Scanning Esca Microprob, Al $K\alpha_1$ radiation). For XPS experiments detecting the changes of the N 1s binding energy, dyes were first adsorbed on

sample Au/TiO_2-0 0 1 followed by centrifugation and separation, and then the solid catalysts were washed to completely remove the physically adsorbed dyes molecules. The washed samples were dried in a vacuum at room temperature. The above process was carried out in the dark to ensure that no photoreaction would occur during the sample treatment. The infrared spectra of dyes adsorbed on the catalysts were obtained by a Nicolet Nexus 670 Fourier transform infrared (FT-IR) spectrometer at a resolution of 4 cm^{-1}. A total of 64 scans were performed to obtain each spectrum. The samples used in this experiment were prepared by the same method as that in the XPS measurements. The electrophoretic mobility of Au/TiO_2-0 0 1 particles in aqueous suspensions (0.1 g/L) was measured to determine its ζ-potential as a function of pH using a Zetasizer 3000 instrument (Malvern Co., UK) at 25 °C. Diffuse reflection spectra (DRS) of the samples were recorded on a Varian Cary-500 spectrophotometer. Electron spin resonance (ESR) signals were recorded with a Bruker A300 spectrometer. The photoluminescence spectra were surveyed by Edinburgh FL/FS900 spectrometer. In particular, the generation of hydroxyl radicals in solution was detected by the photoluminescence (PL) technique with terephthalic acid (TA) as a probe molecule. The detailed experimental procedure was similar to that of the photocatalytic activity test except that the dye aqueous solution was replaced by the 5×10^{-3} M TA aqueous solution containing a concentration of 0.01 M NaOH. A 300 W Xe lamp (Beijing Trustech, PLS-SXE300c) with a 420 nm cut-off filter was used as a light source.

2.5. Photocatalytic activity measurement

Photocatalytic degradation of Rhodamine B (RhB) was conducted in a beaker at room temperature. 80 mg photocatalysts were added to the beaker containing 80 ml RhB aqueous solution with the initial concentration of 2×10^{-5} M. Prior to irradiation, the solution was magnetically stirred in the dark for 1 h to ensure the establishment of an adsorption–desorption equilibrium between photocatalyst and RhB dye. Then, the suspension was irradiated under a 300 W Xe lamp with a 420 nm cut-off filter from top of beaker. At given time intervals, 2 ml suspensions were sampled and centrifuged to remove photocatalyst powders, and then the filtrates were analyzed by Diffusive Reflective UV-vis spectroscopy (Varian Cary-50).

2.6. Photoelectrochemical measurements

The indium-tin oxide (ITO) glasses, as working electrode, were cleaned by sonication in cleanout fluid, acetone and ethanol for 10 min, respectively. 10 mg photocatalyst powder was dispersed into 0.5 ml dimethylformamide under sonication for 6 h to get slurry. The as-prepared slurry spread onto the conductive surface of ITO glass to form a photocatalyst film with the area of 0.25 cm^2. Subsequently, uncoated parts of the ITO glass were isolated with epoxy resin.

Photocurrent was measured by the conventional three-electrode electrochemical cell with a working electrode, a platinum foil counter electrode and a saturated calomel electrode (SCE) as reference electrode. The working electrode was immersed in a sodium sulfate electrolyte solution (0.2 M) and irradiated by a 300 W xenon lamp with a 420 nm cut-off filter from the back side in order to minimize the influence of thickness of the semiconductor layer. The light/dark short circuit photocurrent response was recorded with a BAS Epsilon workstation.

Electrochemical Impedance Spectroscopy (EIS) experiment was carried out on a ZENNIUM electrochemical workstation (Zahner, Germany). EIS was used to evaluate the properties of different photocatalysts under AC polarization, and was conducted in a frequency range of 200 kHz to 5 mHz for an amplitude of 10 mV in DC potential of Open Circuit Potential (OCP) after a 10 min delay.

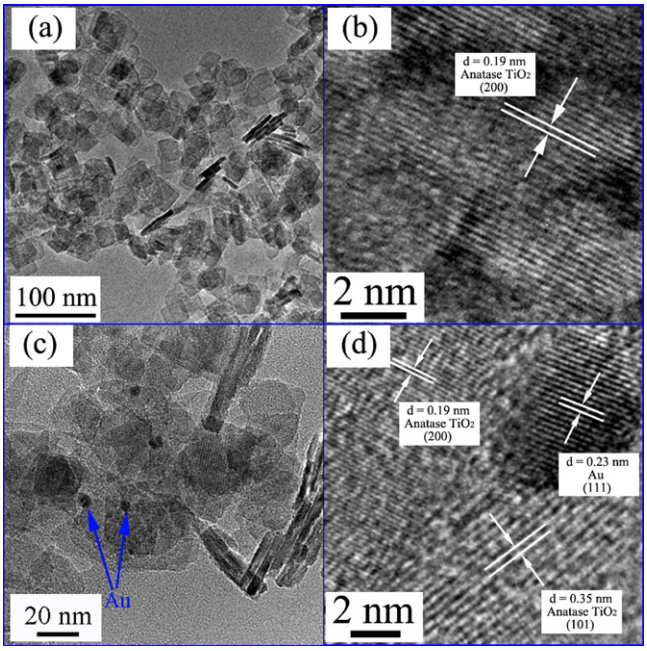

Fig. 1. TEM and HRTEM images of the samples with loading (c and d) 1 wt.% Au and without (a and b) Au.

3. Results and discussion

3.1. Characterization of Au/TiO_2-0 0 1

3.1.1. Morphology and phase structures

The TiO_2 nanosheets with dominant exposed {0 0 1} facets (denoted as TiO_2-0 0 1) were successfully synthesized by hydrothermal method. The TEM and XRD were employed to investigate the morphology and crystal structure of as-prepared TiO_2 nanosheets, respectively. The TEM image of TiO_2-0 0 1 nanocrystal (in Fig. 1a) shows that typical morphology of as-prepared TiO_2 made up of nanosheets, which have an average thickness of 3 nm versus 30 nm in lateral size. According to the symmetries of anatase TiO_2 [7,9,38], the two flat square surfaces can be ascribed to {0 0 1} facets of anatase TiO_2 nanosheets. Fig. 1b is a HRTEM image of TiO_2-0 0 1, which shows that the lattice spacing is ca. 0.19 nm, corresponding to the (2 0 0) lattice planes of anatase TiO_2. On the basis of the structure information [5,39], the top and bottom of truncated bipyramid can be assigned to highly reactive {0 0 1} facets of anatase TiO_2, which indicates that the exposed facet of TiO_2-0 0 1 is (0 0 1) facet. After the Au NPs supported on the TiO_2 nanosheets, the morphology and microstructure of the sample were also identified by TEM and HRTEM, as shown in Fig. 1c and d, respectively. TEM image of Au/TiO_2-0 0 1 reveals that irregular morphology, the same as the bare TiO_2-0 0 1, made of the agglomerates of nanosheets with length of ~30 nm and well-dispersed Au NPs formed. Three kinds of lattice fringes with *d* spacing of about 0.35, 0.19 and 0.23 nm were observed by HRTEM (Fig. 1d), which can be indexed as the (1 0 1) and (2 0 0) plane of anatase TiO_2, as well as the (1 1 1) plane of face-centered cubic Au, respectively. In addition, the HRTEM image (Fig. 1d) also confirms that these Au nanoparticles are well-dispersed and have an average diameter of ca. 5.0 nm.

Fig. 2 shows the XRD patterns of the parent TiO_2-0 0 1 and the Au/TiO_2-0 0 1 samples. All diffraction peaks (Fig. 2a) can be well indexed to anatase phase (JCPDS No. 21-1272, space group:

Table 1
Effects of Au_x on the physical properties and photocatalytic activity of samples.

Sample	Au content (wt.%)	Crystal size[a] (nm)	A_{BET}[b] (m^2/g)	Pore volume (cm^3/g)	Average pore size (nm)	k_{RhB}[c] (h^{-1})
TiO_2-0 0 1	0	15.9	121	0.37	12.4	0.54
$Au_{0.5}/TiO_2$-0 0 1	0.5	15.0	119	0.36	12.2	1.68
$Au_{1.0}/TiO_2$-0 0 1	1.0	15.9	108	0.34	12.1	3.00
$Au_{2.0}/TiO_2$-0 0 1	2.0	14.8	105	0.30	11.6	0.84

[a] The crystal sizes are calculated by the Scherrer's equation.
[b] The specific surface area.
[c] The reaction rate constant of RhB degradation.

$I4_1/amd$) present in both the bare TiO_2-0 0 1 and the Au/TiO_2-0 0 1 samples, indicating that the as-prepared TiO_2 nanosheets and Au supported TiO_2 nanosheets are pure anatase TiO_2 nanocrystals. The average crystal sizes of bare TiO_2-0 0 1 and the Au/TiO_2-0 0 1 are estimated by using the Scherrer's equation on the anatase (1 0 1) diffraction peak at $2\theta = 25.3^\circ$, the results are listed in Table 1. All the samples have almost the same crystallite size, implying that the deposition of Au does not evidently alter the crystalline phase and crystallite size of TiO_2 nanosheets. No diffraction peaks arising from Au are observed. This reconfirms that Au is dispersed highly on the surface of TiO_2 nanosheets.

3.1.2. N_2-sorption

Fig. S1 (in the supporting information) shows nitrogen adsorption–desorption isotherms and the corresponding pore-size distribution curves (inset in Fig. S1) of the bare TiO_2-0 0 1 and the Au/TiO_2-0 0 1 samples. It can be observed apparently that the nitrogen adsorption–desorption isotherms of bare TiO_2-0 0 1 sample is of the type IV according to IUPAC classification. The loop ring of the Au/TiO_2-0 0 1 sample is able to overlap with that of the TiO_2-0 0 1 sample, and no obvious change on the pore size distribution has been observed. It indicates that Au loading does not destroy the porous structure of TiO_2 nanosheets, which consists with the XRD and TEM results. In order to clearly see the variations of samples before and after Au loaded, the BET surface area, pore volume and average pore size of the samples (bare TiO_2-0 0 1 and Au_x/TiO_2-0 0 1 with different Au loading) obtained from nitrogen sorption are summarized in Table 1. The BET surface area, pore volume, and average pore size of bare TiO_2-0 0 1 is equal to 121 m^2/g, 0.37 cm^3/g and 12.4 nm, respectively. After Au supported on surface of TiO_2-0 0 1, the BET surface area, pore volume, and average pore size of samples are decreased with the increasing of the content of Au. This is mainly because a part of pores of TiO_2 nanosheets may be blocked by the loaded Au nanoparticles.

3.1.3. UV-vis DRS spectroscopy

The diffuse reflectance spectra of the bare TiO_2-0 0 1 and the Au/TiO_2-0 0 1 are shown in Fig. 3. It can be apparently observed that the Au/TiO_2-0 0 1 samples have a stronger absorption in the visible light region compared with the bare TiO_2-0 0 1 sample, which is due to the SPR effect of Au deposited on TiO_2-0 0 1 surface. The absorption peak at ca. 546 nm is assigned to the characteristic SPR peak of Au NPs. With increasing the content of Au, the absorption intensity of Au SPR peak would be significantly enhanced. This ensures the Au/TiO_2-0 0 1 photocatalysts work under visible light irradiation. For all samples, the optical absorption thresholds of band gap transition on TiO_2 are almost the same before and after Au depositing, indicating that Au only deposits on TiO_2-0 0 1 surface instead of doping into the crystal lattice of TiO_2-0 0 1.

3.1.4. XPS analysis

To illustrate the surface composition and chemical state of the Au/TiO_2-0 0 1 photocatalyst, the Au/TiO_2-0 0 1 samples were characterized by the XPS analysis, as shown in Fig. 4. The sample surface contains C, O, Ti, F and Au elements according to the XPS survey spectra (see Fig. S2). The C 1s peak at ca. 284.6 eV results from the surface adventitious carbon, and the peak at the binding energy of 286.0 eV can be assigned to C—C bond originated from adsorbed butanoxide species (Fig. S3). The high-resolution XPS spectra of the Ti 2p and O 1s of sample are presented in Fig. 4b and c. The peaks located at ca. 458.8 and 464.5 eV in Fig. 4b correspond to Ti $2p_{3/2}$ and Ti $2p_{1/2}$ of TiO_2, respectively, which are identical with the reported values [40]. The O 1s spectrum (Fig. 4c) shows that the curve could be deconvoluted into two peaks, located at 531.4

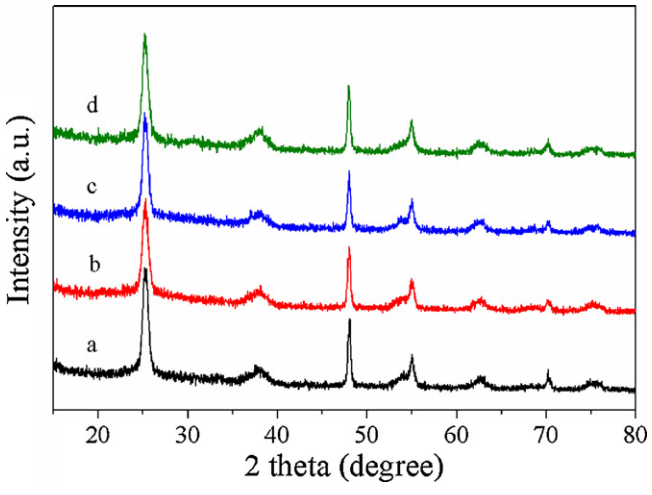

Fig. 2. XRD patterns of pure TiO_2 and Au_x/TiO_2-0 0 1 ($x = 0.5$, 1.0, 2.0) samples obtained with different concentrations of Au: (a) TiO_2-0 0 1; (b) $Au_{0.5}/TiO_2$-0 0 1; (c) $Au_{1.0}/TiO_2$-0 0 1; (d) $Au_{2.0}/TiO_2$-0 0 1.

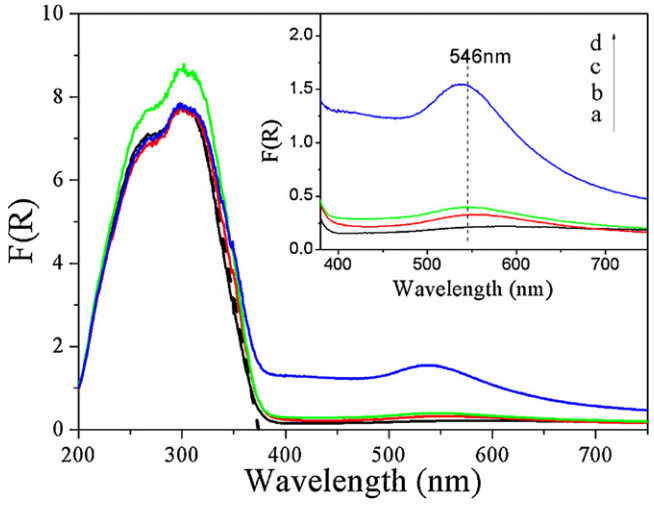

Fig. 3. UV–vis absorbance spectra for the bare TiO_2 and TiO_2 modified with gold nanoparticles: (a) TiO_2-0 0 1; (b) $Au_{0.5}/TiO_2$-0 0 1; (c) $Au_{1.0}/TiO_2$-0 0 1; (d) $Au_{2.0}/TiO_2$-0 0 1.

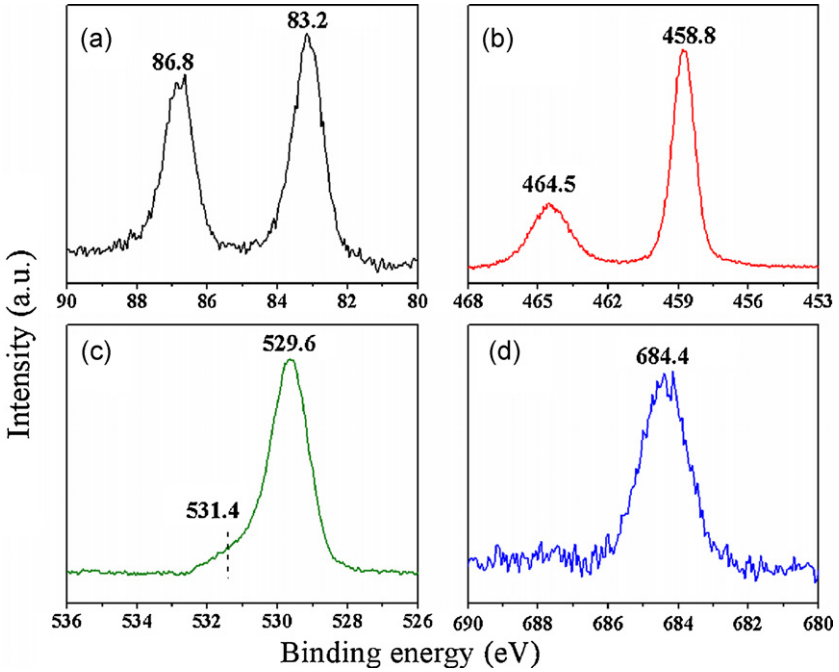

Fig. 4. XPS spectra of $Au_{1.0}/TiO_2$-0 0 1: (a) Au 4f, (b) Ti 2p, (c) O 1s, and (d) F 1s.

and 529.6 eV, respectively. The higher binding energy (BE) peak is attributed to surface adsorbed oxygen, such as hydroxyl species. The lower BE peaks correspond to the O (1s) core level of the O^{2-} anions in the TiO_2 crystal lattice. To facilitate and realize the formation of predominantly (0 0 1) surface, hydrofluoric acid solution was added in reaction system to substantially stabilize unsaturated titanium by the bonding of F-Ti in the TiO_2 crystal growth process [41]. The chemical state of F and the formation of F-Ti species are proved by the F 1s XPS. As shown in Fig. 4d, the peak of F 1s at binding energy of 684.0 eV belonged to the F-Ti species [38] is observed. For Au, the core lines are fixed at 83.2 eV (Au $4f_{7/2}$) and the spin orbit separations (Δ) are 3.6 eV (Fig. 4a). These results show that the oxidation states of Au on TiO_2-0 0 1 are Au^0 [40,42,43]. Moreover, the binding energy of Au $4f_{7/2}$ is lower than that in the pure Au foil (84.0 eV), which is similar with the results reported by Li et al. [44]. It demonstrates that the negative shift of the Au $4f_{7/2}$ binding energy is due to a strong metal-support interaction. The causes for such a negative shift of the Au $4f_{7/2}$ binding energy have also been discussed by Kruse and Chenakin [45]. They considered that Au nanoparticles in the Au/TiO_2 catalyst were slightly negatively charged due to the electron transfer from oxygen vacancies of the TiO_2, leading to lower the Au $4f_{7/2}$ core-level binding energy in Au/TiO_2. This interaction between Au and TiO_2 would be beneficial for the enhancement of the photocatalytic activity over Au/TiO_2-0 0 1.

3.2. Photoelectrochemical behaviors of Au/TiO_2-0 0 1

The transient photocurrent responses were carried out to distinguish the variations of photoelectric response before and after decorating the Au NPs on TiO_2-0 0 1 nanosheets. Compared with the bare TiO_2-0 0 1 sample, Au/TiO_2-0 0 1 sample exhibits a 3-fold increase in the photocurrent under visible light irradiation (Fig. 5a). The photocurrent spectrum indicates that the electron–hole lifetime at the metal-semiconductor interface is prolonged, and the efficiency of the electron–hole separation has been increased [46]. For the TiO_2-0 0 1 sample, it also exhibited low photoelectric respondence under visible light irradiation. This phenomenon can be ascribed to the existence of oxygen vacancies [47] on the

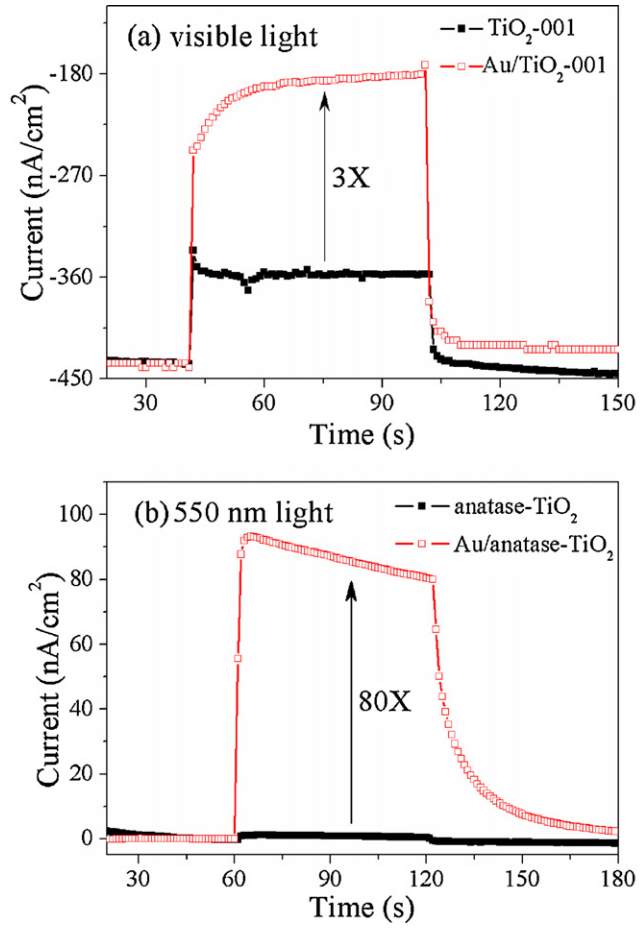

Fig. 5. (a) Photocurrent response of anodic TiO_2-0 0 1 with and without Au nanoparticles at zero bias voltage irradiated with visible ($\lambda \geq 420$ nm) light for 60 s. (b) Comparison of the photocurrent response of anodic commercial anatase TiO_2 with and without Au nanoparticles at 400 mV bias voltage irradiated with $\lambda = 550$ nm light for 60 s.

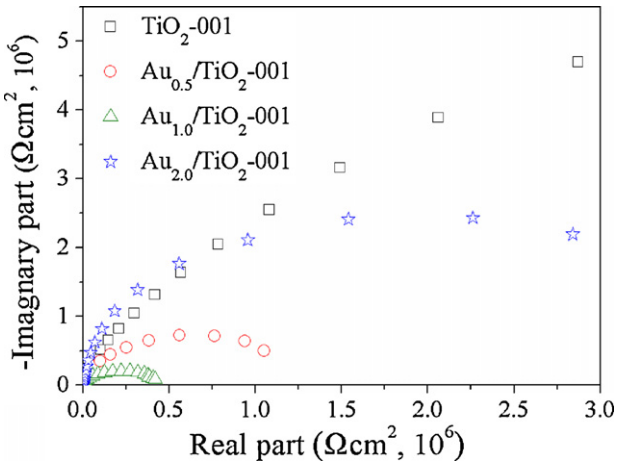

Fig. 6. Nyquist plots for Au_x/TiO_2-0 0 1 (x = 0.5, 1.0, 2.0) samples.

surface of the TiO_2-0 0 1 photocatalyst, which are also confirmed by EPR results (Fig. S4).

To exclude the effect of the defect and clarify the SRP effect of Au NPs on TiO_2, we have also investigated the photocurrent of the commercial anatase TiO_2 with low defects before and after Au deposited under visible light irradiation. As shown in Fig. 5b, the bare TiO_2 shows very low photocurrent response under 550 nm light irradiation (0.15 W/cm^2) because anatase TiO_2 cannot be excited by the incident light. However, a significant photoelectric response on the Au/TiO_2 sample has been observed. In the steady stage, the photocurrent density of the Au/TiO_2 sample is about 80 nA/cm^{-2} under the same condition. It is nearly up to 80-fold increase in the photocurrent as a result of Au NPs. These results strongly demonstrate that the photocurrent enhancement is mainly caused by the SPR effect of Au NPs under visible light irradiation and the lifetime of the photogenerated charge carries has been prolonged on Au/TiO_2 sample efficiently. Meanwhile, they also suggest that the Au/TiO_2 would be a promising visible-light drived photocatalyst.

Fig. 6 shows the Nyquist plots of TiO_2-0 0 1 and Au/TiO_2-0 0 1 electrodes under dark conditions. The diameter of the arc radius on the Nyquist plots of the Au/TiO_2-0 0 1 electrodes is smaller than that of the bare TiO_2-0 0 1 electrode. It reveals that the Schottky junctions formed between Au and TiO_2-0 0 1 can facilitate the separation of photogenerated carriers as well as the interfacial transfer of carriers.

3.3. Visible light induced photocatalytic activity

The above-mentioned discussions indicate that Au/TiO_2-0 0 1 sample may be used as a good candidate for photocatalytic reactions under visible light irradiation. Therefore, the photocatalytic activities of the samples were evaluated by degrading RhB under visible light irradiation. The temporal concentration changes of RhB aqueous solution, determined by UV–vis spectra, during the photocatalytic degradation reaction over the Au/TiO_2-0 0 1 photocatalyst are presented in Fig. 7a. It can be clearly seen that the intensity of absorption band at 554 nm assigned to RhB obviously decreases with a gradual hypsochromic shifts over Au/TiO_2-0 0 1 photocatalyst. The changes of dye concentration and wavelength shift of absorption band with irradiation time are shown in Fig. 7b. The wavelength shift increases with increasing irradiation time and reaches a maximum at 40 min. These results indicate that RhB is first de-ethylated in a stepwise manner within 40 min irradiation and then its conjugated structure is destroyed [48,49]. Fig. 9 shows that the photolysis of RhB can be negligible. Moreover, the concentration of RhB does not change in the presence of the catalysts under dark conditions. Therefore, the presence of both visible light and photocatalyst are necessary for the photocatalytic reaction to proceed.

The stability of the plasmonic Au/TiO_2-0 0 1 photocatalyst was evaluated by performing the recycle experiments of the photocatalyst under similar conditions (Fig. S5). After five recycles, the photocatalytic activity did not decrease apparently, which indicated the photocatalyst possessed high activity stability for degrading RhB. Moreover, the crystal structure of Au/TiO_2-0 0 1 after 5th run was also checked by XRD (Fig. S6), which revealed no observable change after the reaction.

To investigate why the RhB on the surface of Au_x/TiO_2-0 0 1 underwent a gradually N-de-ethylation process, the interaction between the dye and the catalyst has been studied. It is known that the N 1s binding energy is very sensitive to the chemical environment of the -N (Et)$_2$ group and XPS technique provides an efficient method for the study on interaction modes of RhB with the photocatalyst. Fig. 8a shows the N 1s XPS spectra of RhB on Au/TiO_2-0 0 1. When the RhB anchors strongly on the surface of TiO_2 via the carboxylic (—COOH) group, the binding energy of N 1s maintains 399.7 eV [50]. However, the N 1s binding energy of RhB on the Au/TiO_2-0 0 1 surface is 400.6 eV, which is higher than that of pure RhB (399.7 eV). The result suggests that the chemical environment of nitrogen is markedly different between these two systems, that is, the -N (Et)$_2$ group absorb on the surface of the Au/TiO_2-0 0 1 by the -N (Et)$_2$ group instead of the carboxylic (—COOH) group so that the RhB molecule is chemically adsorbed on the Au/TiO_2-0 0 1 surface. This would cause the RhB underwent a rapid N-de-ethylation process on the surface of Au/TiO_2-0 0 1. The FT-IR spectra are expected to give more information on the interaction between the dye and the surface of the catalyst. Fig. 8b displays the FT-IR spectra of the Au/TiO_2-0 0 1 before and after absorption of RhB. Obviously, after adsorption of RhB on the surface of Au/TiO_2-0 0 1, a new vibration band appeared at 1150 cm^{-1}. The fact suggests that the RhB has interaction with the surface of Au/TiO_2-0 0 1. In addition, the result of zeta potential measurement reveals that the surface of Au/TiO_2-0 0 1 is dominated by negative charges in neutral solutions (Fig. S7). Therefore, it is easy for the surface of Au/TiO_2-0 0 1 to absorb the positive-charged diethylamine group of RhB.

In order to optimize the reaction condition and gain some insights into the plasmonic photocatalytic activity of RhB degradation over the Au/TiO_2-0 0 1 photocatalyst, the effects of Au content, the calcination temperature of TiO_2-0 0 1, the supporter, and the reaction atmosphere on photocatalytic degradation of RhB under visible light irradiation are investigated in detail.

3.3.1. Effect of the Au content

The Au_x/TiO_2-0 0 1 photocatalysts with different Au content were prepared to examine the effect of Au content on photocatalytic degradation of RhB under visible light irradiation. Fig. 9 shows the photodegradation of RhB over the Au_x/TiO_2-0 0 1 (x = 0, 0.5, 1.0, 2.0) with different Au content and N doped TiO_2 photocatalysts. It can be concluded that the RhB molecules are degraded in the presence of TiO_2-0 0 1 under visible light irradiation and in fact the photodegradation conversion of RhB is about 40% after irradiation for 80 min. According to the previous report [41], we consider that the visible light induced photoactivity for the bare TiO_2-0 0 1 can be attributed to the self-photosensitized effect of RhB molecules. After supporting Au NPs on the surface of TiO_2-0 0 1, the Au/TiO_2-0 0 1 photocatalysts show much higher photocatalytic activity than the bare TiO_2-0 0 1 for the degradation of RhB in aqueous solution, and the $Au_{1.0}/TiO_2$-0 0 1 photocatalyst exhibits the highest photocatalytic efficiency among all the samples. Additionally, the comparison experiment is conducted to further evaluate the photocatalytic performance of Au/TiO_2-0 0 1.

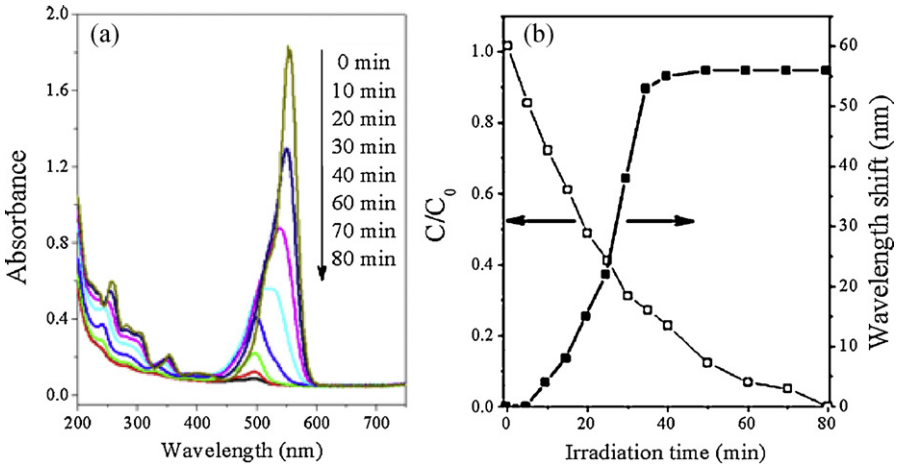

Fig. 7. (a) Changes in UV–vis absorption spectra of RhB aqueous solutions under visible-light irradiation in the presence of $Au_{1.0}/TiO_2$-0 0 1 composite samples. (b) Absorbance changes in the major absorption band (hollow) and the corresponding wavelength shifts (solid) of the spectra of RhB solutions over $Au_{1.0}/TiO_2$-0 0 1.

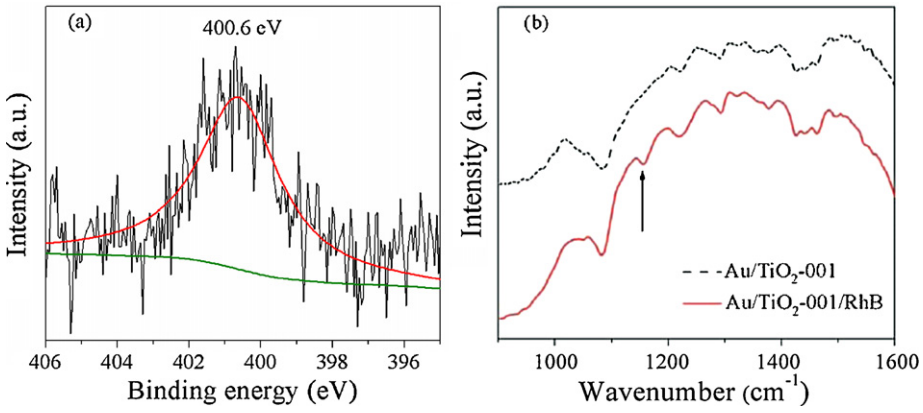

Fig. 8. (a) The N 1s XPS spectra of RhB over Au/TiO_2-0 0 1. (b) The IR spectra of the Au/TiO_2-0 0 1 and Au/TiO_2-0 0 1/RhB.

Importantly, the photocatalytic activity of Au/TiO_2-0 0 1 is significantly higher than that on N doped TiO_2, a popular visible-light responsive photocatalyst. The kinetics of RhB degradation under visible light irradiation for all samples is presented in Fig. S8. The RhB photodegradation over the catalysts follows a pseudo first-order reaction. As shown in Table 1, the corresponding apparent degradation rate constants for TiO_2-0 0 1, N/TiO_2, $Au_{0.5}/TiO_2$-0 0 1, $Au_{1.0}/TiO_2$-0 0 1 and $Au_{2.0}/TiO_2$-0 0 1 are estimated to be 0.54 h^{-1}, 0.60 h^{-1}, 1.68 h^{-1}, 3.00 h^{-1} and 0.84 h^{-1}, respectively. It can be seen that the photocatalytic reaction rate constants follow the order $Au_{1.0}/TiO_2$-0 0 1 > $Au_{0.5}/TiO_2$-0 0 1 > $Au_{2.0}/TiO_2$-0 0 1 > N/TiO_2 > TiO_2-0 0 1. Although the Au loading can efficiently increase the photocatalytic activity of TiO_2-0 0 1, the excess Au NPs would significantly reduce the reaction activity. This decreased activity may be caused by the integrative effect of the Au NPs aggregation and the active sites covering by the excess Au [19,24,35].

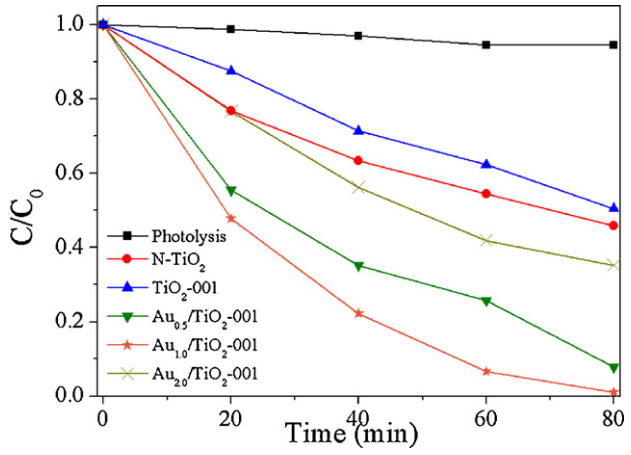

Fig. 9. The photodegradation of RhB over the Au_x/TiO_2-0 0 1 (x = 0, 0.5, 1.0, 2.0) with different Au loading and N doped TiO_2 photocatalysts.

3.3.2. *Effect of the calcination temperature of TiO_2-0 0 1*

In order to distinguish the effect of the exposed percent of (0 0 1) facets on the photocatalytic activities, the as-prepared TiO_2-0 0 1 have been calcined at different temperatures (the samples are denoted by TiO_2-0 0 1-*T*, where *T* is calcination temperature). Fig. S9 shows the XRD patterns of TiO_2-0 0 1 prepared by hydrothermal reaction at 180 °C for 24 h, followed a calcined process. The crystalline phase of TiO_2-0 0 1 maintains the anatase phase even the calcination temperature up to 600 °C. When the temperature reaches 800 °C, the TiO_2-0 0 1 is completely transformed into rutile TiO_2. Meanwhile, the crystallinities of these samples are obviously improved with increasing calcination temperature, while their BET surface areas of the samples are reducing (Table 2). The morphologies of these samples are also characterized by TEM technique. As shown in Fig. S10, the TiO_2 nanosheets are accumulated to form

Table 2
Effects of the calcination temperature on the physical properties and photocatalytic activity of samples.

Sample	Calcination temperature (°C)	A_{BET}[c] (m^2/g)	k_{RhB}[d] (h^{-1})	k'_{RhB}[e] ($g\,h^{-1}\,m^{-2}$, $\times10^{-3}$)
Au/TiO_2-001	Uncalcined[a]	108.0	3.00	27.8
Au/TiO_2-001-400	400[b]	33.7	0.66	19.6
Au/TiO_2-001-600	600[b]	26.1	0.42	16.1
Au/TiO_2-001-800	800[b]	18.5	0.30	16.2

[a] TiO_2-001 prepared by hydrothermal reaction at 180 °C for 24 h.
[b] TiO_2-001 prepared by hydrothermal reaction at 180 °C for 24 h, followed a calcined process.
[c] The specific surface area.
[d] The reaction rate constant of RhB degradation.
[e] The k'_{RhB} values were k_{RhB} values normalized with the surface area, respectively.

large nanoparticles as increasing the calcination temperature and the exposed percent of (001) facet has been decreased. Fig. 10 shows their photocatalytic activities for degradation of RhB under visible light irradiation. Obviously, the degradation rates of RhB over these photocatalysts decreased gradually with the ascending of the calcination temperature of TiO_2-001. It may be owing to the decrease of both its BET surface area and the proportion of its (001) facet. To find out the main factor accounting for this phenomenon, we normalize the photocatalytic degradation rates with the surface areas to rule out the effect of surface areas on their photocatalytic activities. After comparing the degradation rates of RhB before and after normalizing with the surface areas, we find that the order of the normalized rates is similar to that of the original ones. The result confirms that increasing the {001} facets exposed surface area can enhance the photocatalytic activity efficiently. In addition, the normalized rate of RhB degradation on Au/TiO_2-001-800 is the same as that of Au/TiO_2-001-600 although its original rate was the lowest among all samples, which illustrated that the photocatalytic reaction is derived from the photogenerated electrons of Au NPs. Therefore, the smaller surface area of Au/TiO_2-001-800 could be mainly responsible for its original poor activity, while the relatively higher normalized degradation rate could be related to its appropriate conduction band level. So it is reasonable that Au/TiO_2-001 with the largest surface area possesses the highest original photocatalytic activity. Therefore, we consider that the reduction of surface area and {001} exposed surfaces of the TiO_2-001 nanosheets is the key factors for the decrease of photocatalytic activity with increasing calcination temperature.

3.3.3. Effect of the supporter

Fig. 11 shows the comparison of photocatalytic performance of four Au/TiO_2 photocatalysts with different supporter (TiO_2-001, P25 (Degussa, 80% anatase TiO_2 and 20% rutile TiO_2), anatase TiO_2 and rutile TiO_2). The photocatalytic activities for these samples follow a trend: Au/TiO_2-001 > Au/P25 > Au/anatase TiO_2 > Au/rutile TiO_2. The result reveals that the crystalline phase of TiO_2 is an important factor for photodegradation of RhB over Au/TiO_2 under visible light irradiation. Furthermore, the photocatalytic activities of Au/TiO_2-001 are much higher than that of Au/anatase TiO_2 which dominated by {101} facets, indicating the photocatalytic activities are strongly associated with the surface structures of the exposed crystal facets and the (001) facet may be the predominance active facet. The TiO_2 nanosheets with exposed {001} facets can enhance the adsorption of pollutant molecules due to their higher reactivity and high surface energy [11], and the absorbed RhB can be quickly reacted with the active species, which results in the higher photocatalytic activity. This is in agreement with the above results reported in Section 3.3.2. Interestingly, the photocatalytic activity of Au/TiO_2-001 is also higher than that of Au/P25, where the heterojunction between anatase and rutile TiO_2 exists to accelerate the mobility of injected photogenerated electron. It reconfirms that the enhancement of {001} facets exposed surface area is an efficient method to increase the photocatalytic activity of Au/TiO_2 under visible light irradiation.

3.3.4. Effect of the reaction atmosphere

In the previous reports [51], •OH, $•O_2^-$ and h^+ are commonly suggested as the primary active species in the photocatalytic redox reactions. It is interesting to determine the active species in the photocatalytic reaction process over Au/TiO_2-001. To clarify which active species dominates the photocatalytic degradation of RhB, the reactions were carried out in different reaction atmospheres firstly.

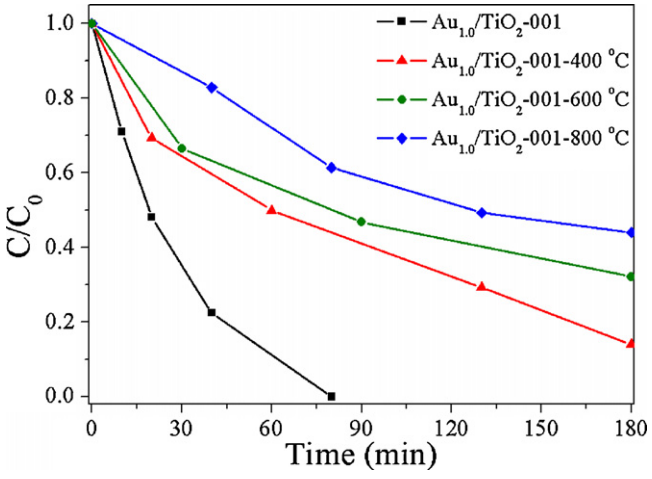

Fig. 10. Effects of the calcination temperature of TiO_2-001 on photocatalytic degradation of RhB under visible light irradiation.

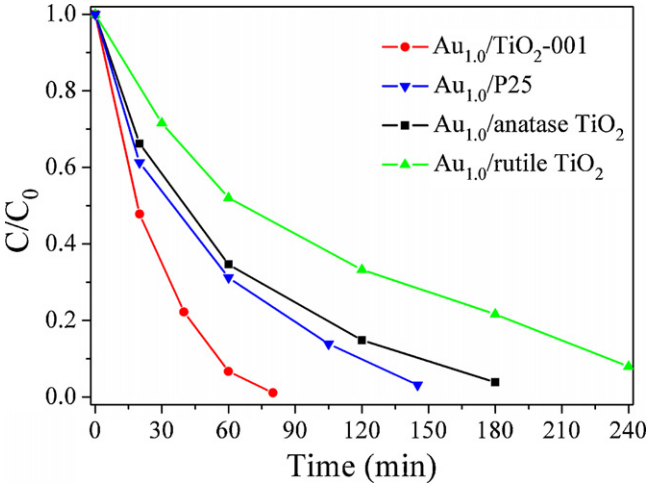

Fig. 11. Comparison of photocatalytic performance of the four Au/TiO_2 photocatalysts with different support ($Au_{1.0}$/TiO_2-001, $Au_{1.0}$/P25, $Au_{1.0}$/anatase TiO_2 and $Au_{1.0}$/rutile TiO_2).

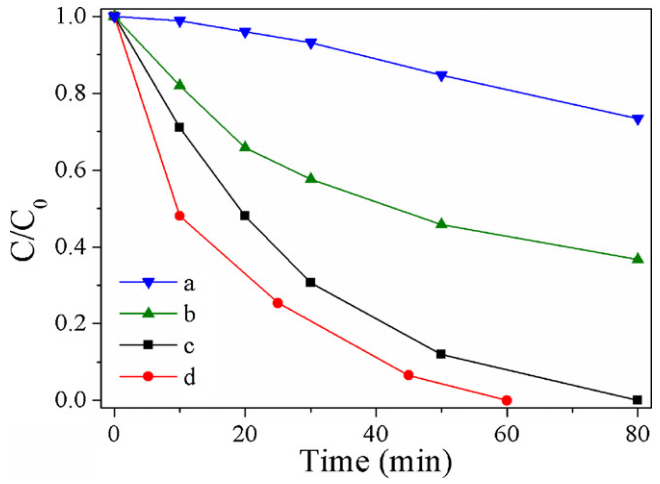

Fig. 12. Variations in the concentration of RhB over photocatalysts under the different reaction atmospheres under visible light irradiation: (a) in the presence of TiO_2-0 0 1 bubbling with N_2; (b) in the presence of $Au_{1.0}/TiO_2$-0 0 1 bubbling with N_2; (c) in the presence of $Au_{1.0}/TiO_2$-0 0 1 under the saturated air; (d) in the presence of $Au_{1.0}/TiO_2$-0 0 1 bubbling with O_2.

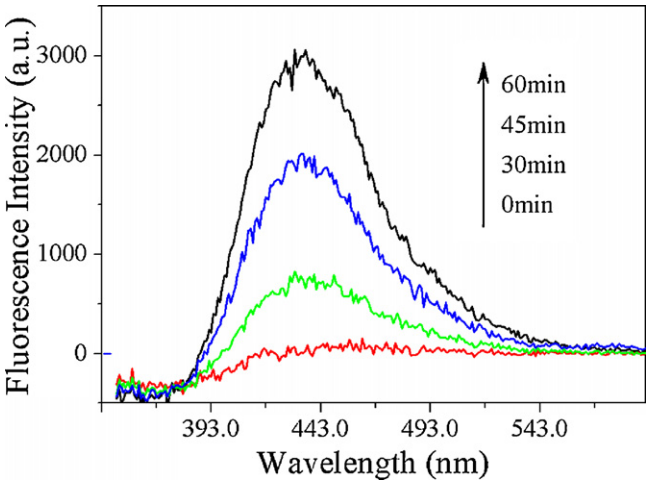

Fig. 13. PL spectra of terephthalic acid solution with $Au_{1.0}/TiO_2$-0 0 1 sample under visible-light irradiation.

Fig. 12 shows the photocatalytic degradation of RhB over Au/TiO_2-0 0 1 in saturated air, N_2 and O_2. It can be clearly observed that the photocatalytic activities are quite different. In N_2 atmospheres, only the active species hole (h^+) is formed under visible light irradiation. For •OH radicals, due to relatively low oxidative potential of h^+ (E^0 = +0.6 eV), the •OH radicals cannot be formed via oxidizing adsorbed hydroxyl species (E^0 (•OH/H_2O) = +2.3 eV) [52]. Because the activity of Au/TiO_2-0 0 1 is higher than that of TiO_2-0 0 1 which is caused by the photosensitization effect of RhB, h^+ is one of the active species in the photocatalytic process over Au/TiO_2-0 0 1. In O_2 atmospheres, besides h^+, $•O_2^-$ radicals can be produced by the interaction of adsorbed oxygen with injected electrons in the conduction band. In the presence of O_2, the Au/TiO_2-0 0 1 photocatalyst exhibits a higher photocatalytic activity for photodegradation of RhB. With increasing the concentration of O_2, the photocatalytic activity is further improved. It suggests that the $•O_2^-$ radicals may also be one of the active species in this reaction system with O_2. To confirm the existence of $•O_2^-$ radicals, ESR spin-trapped with DMPO technique has been conducted. Unfortunately, no characteristic peaks of DMPO-$•O_2^-$ adduct have been observed because the $•O_2^-$ radicals concentration may be below the instrument's resolution under the operation conditions. Previous reports indicate the •OH radicals would be produced by deriving from the photogenerated electron-induced multistep reduction of $•O_2^-$ radicals [53]. So, the PL-TA technique with very high sensitivity is used in the detection of •OH radicals to indirectly demonstrate the production of $•O_2^-$ radicals. Fig. 13a shows the PL spectra of terephthalic acid solution under visible-light irradiation with different irradiation time. Clearly, a PL peak at about 425 nm is observed when suspension illuminated by visible light, indicating that •OH produced during photocatalytic reactions [54]. Moreover, PL intensities for samples with different Au content (see in Fig. S11) are different under the same condition. The amount of •OH radicals produced on sample $Au_{1.0}/TiO_2$-0 0 1 is larger than that on other samples. The results confirm that the $•O_2^-$ radicals could be produced in the photocatalytic process and the concentration of $•O_2^-$ radicals on $Au_{1.0}/TiO_2$-0 0 1 is the highest. It is worth to note that the order of $•O_2^-$ radicals concentration is in good parallel with the variation in photocatalytic degradation rate of these photocatalysts. Therefore, we may conclude that RhB is degraded by the oxidation process of $•O_2^-$ and •OH radicals.

3.3.5. *Possible reaction mechanism of Rhodamine B degradation under visible light irradiation*

Base on the experimental results, the possible mechanism for photocatalytic degraded RhB over Au/TiO_2-0 0 1 may be proposed, and is illustrated in Fig. 14. Under visible light irradiation, a charge carrier has been produced by the SPR effect of Au NPs on the TiO_2-0 0 1 surface while it does not happen on the TiO_2 surface. Due to the photogenerated electrons with a more negative potential compared with the conduction band (CB) level of TiO_2-0 0 1, the electrons would transfer from an excited Au NP to a TiO_2 particle. The migration is very fast with a rate less than 240 fs on TiO_2 [55], indicating that the photogenerated electron–hole pairs can be effectively separated. Subsequently, the photocatalytic degradation of RhB adsorbed would start from holes ($•Au^+$) attack. At the same time, the photogenerated electron injected into the conduction band of TiO_2 may be trapped by adsorbed oxygen to form $•O_2^-$ radicals. And then, the $•O_2^-$ radicals can further react with H^+ and the trapped electron to produce H_2O_2 in aqueous solution. The formed H_2O_2 would be transformed into •OH radicals by capturing an electron [41,56]. Finally, the reactants may be destroyed by the forming $•O_2^-$ and •OH radicals. In addition, the adsorbed RhB molecule can be photo-excited to form RhB* radical which may also transfers an electron to the CB of TiO_2 to form $RhB^{•+}$. This photosensitization process would lead to the decomposition of RhB. Therefore, the Au/TiO_2-0 0 1 nanosheets with a high visible-light photocatalytic activity can be assigned to the SPR effect of Au NPs. The high electron mobility may also be one reason for that Au/TiO_2-0 0 1 has the highest activity compared with the other Au/TiO_2 photocatalysts.

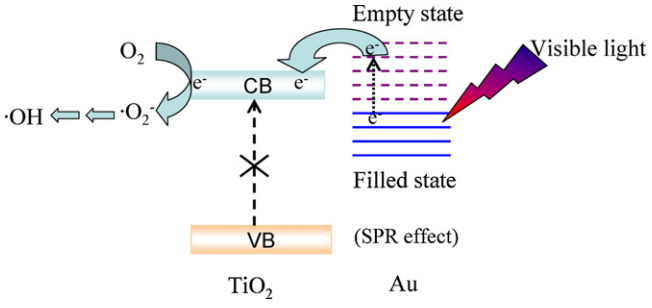

Fig. 14. The possible mechanism for photocatalytic degraded RhB over Au/TiO_2-0 0 1.

4. Conclusion

Novel Au/TiO_2 nanosheet photocatalyst with a high percentage of exposed {0 0 1} facets is successfully prepared by a hydrothermal reaction combining with the polyol reduction process for the first time. TEM and XPS results show that Au in the form of metallic state is uniformly deposited on the TiO_2-0 0 1. Based on the SPR effect of Au, the as-prepared samples exhibit highly photocatalytic activities for degradation of RhB under visible light irradiation. Moreover, the degradation rate of RhB over Au/TiO_2-0 0 1 is much faster than that on the bare TiO_2-0 0 1 and other Au deposited photocatalysts, such as Au/P25, Au/anatase TiO_2 and Au/rutile TiO_2. The obvious enhancement in the visible-light photocatalytic activity is mainly due to the synergetic effects of three factors: (1) the exposure of highly reactive {0 0 1} facets for nanosheets; (2) the higher migration rate of injected electrons from photo-excited Au to (0 0 1) facet compared with the other facets; (3) the more adsorption of pollutant molecules on (0 0 1) facet with high surface energy. By analyzing the results of the controlled experiments, the possible radical species involved in the degradation of RhB are proposed. It is revealed that h^+ plays a predominant role in degradation of RhB aqueous solution without O_2 under visible light irradiation instead of $^{\bullet}O_2^-$ and $^{\bullet}OH$ radicals. While in the presence of O_2, the main active species include h^+, $^{\bullet}O_2^-$ and $^{\bullet}OH$ radicals. In addition, our present work highly suggests that there is still a wide scope to enhance the photocatalytic activity of metal-semiconductor nanocomposites by tuning the exposed facets of the supporters.

Acknowledgments

The work is supported by National Natural Science Foundation of China (U1033603, 20977016 and 21173046), National Basic Research Program of China (973 Program: 2011CB612314 and 2010CB234604), Program for Changjiang Scholars and Innovative Research Team in University (PCSIRT0818).

Appendix A. Supplementary data

Supplementary data associated with this article can be found, in the online version, at doi:10.1016/j.apcatb.2012.02.020.

References

[1] D. Wang, H. Jiang, X. Zong, Q. Xu, Y. Ma, G. Li, C. Li, Chem. Eur. J. 17 (2011) 1275–1282.
[2] F. Seker, K. Meeker, T.F. Kuech, A.B. Ellis, Chem. Rev. 100 (2000) 2505–2536.
[3] X. Han, Q. Kuang, M. Jin, Z. Xie, L. Zheng, J. Am. Chem. Soc. 131 (2009) 3152–3153.
[4] Z. Wang, K. Lv, G. Wang, K. Deng, D. Tang, Appl. Catal. B 100 (2010) 378–385.
[5] H.G. Yang, C.H. Sun, S.Z. Qiao, J. Zou, G. Liu, S.C. Smith, H.M. Cheng, G.Q. Lu, Nature 453 (2008) 638–641.
[6] S. Liu, J. Yu, M. Jaroniec, J. Am. Chem. Soc. 132 (2010) 11914–11916.
[7] X. Wu, Z. Chen, G.Q. Max Lu, L. Wang, Adv. Funct. Mater. 21 (2011) 4167–4172.
[8] F. Amano, O.-O. Prieto-Mahaney, Y. Terada, T. Yasumoto, T. Shibayama, B. Ohtani, Chem. Mater. 21 (2009) 2601–2603.
[9] J. Pan, G. Liu, G.Q. Lu, H.-M. Cheng, Angew. Chem. Int. Ed. 50 (2011) 2133–2137.
[10] G. Liu, C. Sun, H.G. Yang, S.C. Smith, L. Wang, G.Q. Lu, H.M. Cheng, Chem. Commun. 46 (2010) 755–757.
[11] Q. Xiang, J. Yu, M. Jaroniec, Phys. Chem. Chem. Phys. 13 (2011) 4853.
[12] X. Zong, Z. Xing, H. Yu, Z. Chen, F. Tang, J. Zou, G.Q. Lu, L. Wang, Chem. Commun. 47 (2011) 11742–11744.
[13] X. Chen, Z. Zheng, X. Ke, E. Jaatinen, T. Xie, D. Wang, C. Guo, J. Zhao, H. Zhu, Green Chem. 12 (2010) 414.
[14] S. Sun, W. Wang, L. Zhang, M. Shang, L. Wang, Catal. Commun. 11 (2009) 290–293.
[15] H. Zhu, X. Chen, Z. Zheng, X. Ke, E. Jaatinen, J. Zhao, C. Guo, T. Xie, D. Wang, Chem. Commun. (2009) 7524–7526.
[16] Y. Tian, T. Tatsuma, J. Am. Chem. Soc. 127 (2005) 7632–7637.
[17] S. Oros-Ruiz, J.A. Pedraza-Avella, C. Guzmán, M. Quintana, E. Moctezuma, G. del Angel, R. Gómez, E. Pérez, Top. Catal. 54 (2011) 519–526.
[18] J.-J. Chen, J.C.S. Wu, P.C. Wu, D.P. Tsai, J. Phys. Chem. C 115 (2010) 210–216.
[19] Z. Zheng, B. Huang, X. Qin, X. Zhang, Y. Dai, M.-H. Whangbo, J. Mater. Chem. 21 (2011) 9079–9087.
[20] W. Yan, S.M. Mahurin, Z. Pan, S.H. Overbury, S. Dai, J. Am. Chem. Soc. 127 (2005) 10480–10481.
[21] M. Haruta, S. Tsubota, T. Kobayashi, H. Kageyama, M.J. Genet, B. Delmon, J. Catal. 144 (1993) 175–192.
[22] M. Manzoli, A. Chiorino, F. Boccuzzi, Appl. Catal. B 57 (2005) 201–209.
[23] S. Hwang, M.C. Lee, W. Choi, Appl. Catal. B 46 (2003) 49–63.
[24] H. Zhu, X. Ke, X. Yang, S. Sarina, H. Liu, Angew. Chem. Int. Ed. 49 (2010) 9657–9661.
[25] R. Sardar, J.S. Shumaker-Parry, J. Am. Chem. Soc. 133 (2011) 8179–8190.
[26] M.R. Provorse, C.M. Aikens, J. Am. Chem. Soc. 132 (2010) 1302–1310.
[27] O. Lopez-Acevedo, H. Tsunoyama, T. Tsukuda, H. Hakkinen, C.M. Aikens, J. Am. Chem. Soc. 132 (2010) 8210–8218.
[28] C.M. Aikens, J. Phys. Chem. C 112 (2008) 19797–19800.
[29] B. Cojocaru, Ş. Neaţu, E. Sacaliuc-Pârvulescu, F. Lévy, V.I. Pârvulescu, H. Garcia, Appl. Catal. B 107 (2011) 140–149.
[30] C. Burda, X. Chen, R. Narayanan, M.A. El-Sayed, Chem. Rev. 105 (2005) 1025–1102.
[31] R. Bukasov, J.S. Shumaker-Parry, Nano Lett. 7 (2007) 1113–1118.
[32] T.K. Sau, C.J. Murphy, J. Am. Chem. Soc. 126 (2004) 8648–8649.
[33] J.E. Millstone, S. Park, K.L. Shuford, L. Qin, G.C. Schatz, C.A. Mirkin, J. Am. Chem. Soc. 127 (2005) 5312–5313.
[34] F. Kim, J.H. Song, P. Yang, J. Am. Chem. Soc. 124 (2002) 14316–14317.
[35] A.T. Bell, Science 299 (2003) 1688–1691.
[36] M. Valden, X. Lai, D.W. Goodman, Science 281 (1998) 1647–1650.
[37] J. Zeng, Q. Zhang, J. Chen, Y. Xia, Nano Lett. 10 (2010) 30–35.
[38] H.G. Yang, G. Liu, S.Z. Qiao, C.H. Sun, Y.G. Jin, S.C. Smith, J. Zou, H.M. Cheng, G.Q. Lu, J. Am. Chem. Soc. 131 (2009) 4078–4083.
[39] X.H. Yang, Z. Li, C. Sun, H.G. Yang, C. Li, Chem. Mater. 23 (2011) 3486–3494.
[40] P. Lignier, M. Comotti, F. Schüth, J.-L. Rousset, V. Caps, Catal. Today 141 (2009) 355–360.
[41] Q. Xiang, J. Yu, B. Cheng, H.C. Ong, Chem. Asian J. 5 (2010) 1466–1474.
[42] B. Tian, J. Zhang, T. Tong, F. Chen, Appl. Catal. B 79 (2008) 394–401.
[43] J. Huang, W. Dai, H. Li, K. Fan, J. Catal. 252 (2007) 69–76.
[44] H. Li, Z. Bian, J. Zhu, Y. Huo, H. Li, Y. Lu, J. Am. Chem. Soc. 129 (2007) 4538–4539.
[45] N. Kruse, S. Chenakin, Appl. Catal. A: Gen. 391 (2011) 367–376.
[46] D.B. Ingram, S. Linic, J. Am. Chem. Soc. 133 (2011) 5202–5204.
[47] Z. Zhang, X. Wang, J. Long, Q. Gu, Z. Ding, X. Fu, J. Catal. 283 (2011) 202.
[48] J. Zhuang, W. Dai, Q. Tian, Z. Li, L. Xie, J. Wang, P. Liu, X. Shi, D. Wang, Langmuir 26 (2010) 9686–9694.
[49] S. Liang, S. Zhu, Y. Chen, W. Wu, X. Wang, L. Wu, J. Mater. Chem. 22 (2012) 2670–2678.
[50] Q. Wang, C. Chen, D. Zhao, W. Ma, J. Zhao, Langmuir 24 (2008) 7338–7345.
[51] S. Liang, L. Shen, J. Zhu, Y. Zhang, X. Wang, Z. Li, L. Wu, X. Fu, RSC Adv. 1 (2011) 458–467.
[52] S. Liang, X. Wang, Y. Chen, J. Zhu, Y. Zhang, X. Wang, Z. Li, L. Wu, Nanoscale 2 (2010) 2262–2268.
[53] S. Liang, S. Zhu, J. Zhu, Y. Chen, Y. Zhang, L. Wu, Phys. Chem. Chem. Phys. 14 (2012) 1212–1222.
[54] K. Ishibashi, A. Fujishima, T. Watanabe, K. Hashimoto, Electrochem. Commun. 2 (2000) 207.
[55] A. Furube, L. Du, K. Hara, R. Katoh, M. Tachiya, J. Am. Chem. Soc. 129 (2007) 14852–14853.
[56] J. Yu, G. Dai, B. Huang, J. Phys. Chem. C 113 (2009) 16394–16401.